ADVANCED MATERIALS INTERFACES
Open Access
www.advmatinterfaces.de

Stimuli-Responsive Nanoplatforms: ZIF-8-Decorated Ferrocenyl Surfactant-Based Vesicles for Synergistic Therapeutic Applications

*Emin Uysal, Sabiha Gulce Yavas, Gokce Dicle Kalaycioglu, Mustafa Polat, Halil Kalipcilar, and Nihal Aydogan**

One of the most important issues in the design and preparation of drug delivery systems in the recent years is versatility which includes providing synergistic therapeutic effects and sustainability. This study uses a redox-active ferrocenyl surfactant ($FcN^+(CH_2CH_3)_3(CH_2)_{10}CH_3$, $Fc(C_{11})$ where Fc is ferrocene) and pH responsive Zeolitic Imidazolate Framework-8 (ZIF-8) structures to form multifunctional assemblies ($Fc(C_{11})$-AOT/-Rhb@ZIF-8/PDA) that can be used in several application including the drug delivery. The vesicles prepared using AOT-$FC(C_{11})$ constitute the core of the structure. Since the location of the ferrocene group in the molecule structure, which is next to head group, the surface of the vesicles is decorated with the ferrocene group which can act as a Fenton reaction catalyst. The polydopamine (PDA) covered ZIF-8 are used to decorate the surface of the vesicles, creating a truly remarkable structure. The porous structure of ZIF-8 as well as the core of the vesicles can accommodate drug molecules. With the added NIR-responsive character upon PDA coating, this assembled structure can be used for phototermal therapy applications. The properties of this designed multifunctional and multi-responsive system are studied at different pH and under NIR-laser irradiation and show that it has potential to display a triple chemodynamic/ photothermal/ chemotherapeutic effect.

1. Introduction

Engineering solutions in the light of basic science can help to provide better and more sustainable solutions to several health problems. For example, there are many studies on cancer treatment, which still threatens human life today.[1] Due to the complexity and diversity of tumors, the effectiveness of current treatments is diminishing.[2] Currently, studies in tumor therapy have focused on synergistic combined therapies rather than monotherapy.[3] Double and triple combinations of many different types of therapy, such as chemotherapy, immunotherapy, photothermal, photodynamic, and chemodynamic therapies are currently being intensively researched to fight cancer.[2,4] The key to achieve that point is to discover novel combinations of materials that can be used in the production of nanocarriers as a multifunctional tool used in these multiple therapies.

Liposomes or vesicles are well-known and widely used nanocarriers in drug delivery applications due to their ability on controlled release, protection of target molecules from degradation, multiple-drug encapsulation and availability for surface nano-engineering.[5–8] Upon incorporation of a ferrocene-containing surfactant, the formation and disruption of the vesicles can be controlled via redox reactions.[9] In addition, ferrocene is one of the most widely used organometallic compound that can be used for the treatment of cancer and other infectious diseases.[10] It is interesting that the position of ferrocene group within the molecular structure of the surfactant has a vital importance.[11] A surfactant which bears the ferrocene as the head group affect the accessibility of the ferrocene that enables the vesicles to give Fenton reactions. Using H_2O_2 to generate OH radicals which are highly toxic, powerful oxidizing agents, and are widely used especially in advanced oxidation processes,[12] structures containing Fenton agents can be used as chemodynamic therapeutic agents in tumor areas.[13] The transition metal such as Fe^{2+} has been used as a Fenton agent, however, stability problem aggregation and low pH requirement of them limit their use.[14] Ferrocene was used as heterogeneous catalyst for Fenton reactions. The oxidation of

E. Uysal, S. G. Yavas, G. D. Kalaycioglu, N. Aydogan
Department of Chemical Engineering
Hacettepe University
Beytepe, Ankara 06800, Turkey
E-mail: anihal@hacettepe.edu.tr
M. Polat
Department of Physics Engineering
Hacettepe University
Beytepe, Ankara 06800, Turkey
H. Kalipcilar
Department of Chemical Engineering
Middle East Technical University
Ankara 06800, Turkey

The ORCID identification number(s) for the author(s) of this article can be found under https://doi.org/10.1002/admi.202400169

DOI: 10.1002/admi.202400169

Fe^{2+} to Fe^{3+} is reversible reaction and ferrocenenium cation can be reduced back ferrocene using the oxygen.[15–18] Moreover, the Fe^{3+} in ferrocenium moiety can be reduced back to Fe^{2+} by intracellular NAD(P)H, which gives rise to the re-generation of ferrocene which effectively enhances the Fenton reaction as a result improved in-vivo chemodynamic effect can be expected.[19] Since the partition of ferrocene group to aqueous phase is low generally, they are preferred to adsorb to the surface of the porous materials or covalently bound to a polymer backbond.[19,20] Ferrocene containing molecules were also used in drug molecules for combating cancer. Still, none of these uses of ferrocene includes surfactant out of which several colloidal structures can be obtained. This versatility of ferrocene groups makes them not only a drug delivery agent, but also the vesicles out of themselves can replace therapeutic agents. Liposomes can also be integrated into multiple networks using techniques such as layer-by-layer (LbL) assembly.[21] Several materials ranging from the polyelectrolytes to nanoparticles can be used for that purpose.[22] This is considered as another advantage of using the vesicles of ferrocenyl surfactant since synergistic therapy agent needs several effects to be used additively.

Metal-organic frameworks (MOFs) have potential in many applications such as gas separation-storage, sensing and catalysis.[23] However, the ability of MOFs to encapsulate a wide variety of target molecules has brought them to be prominent in medical applications in recent years.[24] Zeolitic imidazolate frameworks (ZIFs), on the other hand, stand out as a subclass of MOFs with a very high potential to carry anticancer drugs with its pH sensitive structure.[25] In this way, ZIFs can be transformed into a synergistic therapy agent as well as being a drug carrier.[26] They have recently been used in many different combinations such as ZIFs with gold[27] and carbon nanoparticles,[28] nucleic acids,[29] metal polyphenol networks,[30] polydopamine and MnO_2 layers[31] on cancer treatment.[1] However, most of these studies are obtained by encapsulating these structures into ZIFs or by modifying the ZIF surfaces.

In this study, for the first time in the literature to the best of our knowledge, we developed vesicles capable of conducting Fenton reactions, a crucial aspect of chemodynamic therapy, by introducing the ferrocenyl surfactant $FcN^{+}(CH_2CH_3)_3(CH_2)_{10}CH_3$ ($Fc(C_{11})$) as the Fenton agent. Its placement within the vesicle bilayer is innovatively utilized with the ferrocene groups situated on the outer surface of the vesicles. This configuration not only preserved the aqueous core for potential pharmaceutical agents but also allowed for surface modification and Fenton reactions. Moreover, our study marks the first instance in literature of utilizing ferrocene-bearing surfactants in both monomeric and aggregate forms, such as micelles or vesicles. Further, we achieved catanionic vesicles using cationic $Fc(C_{11})$ and anionic sodium dioctylsulfosuccinate (AOT), with methylene blue removal method and electron spin resonance (ESR) spectroscopy validating the Fenton reaction efficacy.

Subsequently, we synthesized and functionalized ZIF-8 as a potential drug carrier capable of pH-sensitive cargo release. Coating ZIF-8 with polydopamine (PDA) facilitated its use as a photothermal therapy agent, enhancing therapeutic synergies. Finally, we combined catanionic $Fc(C_{11})$-AOT vesicles and PDA-coated ZIF-8 crystals via electrostatic interactions, yielding a multifunctional drug delivery system with chemodynamic, photothermal, and chemotherapeutic capabilities[32] (see **Scheme 1**). The encapsulation of Rhodamine B within ZIF-8 demonstrates a novel approach, presenting a multitasking application unprecedented in the literature. Leveraging the layer-by-layer (LbL) technique for ZIF-8 and vesicle assembly opens avenues for future research, offering the flexibility to incorporate diverse functional layers.

2. Results and Discussion

Catalytic Activity of N,N-dimethylferrocenylmethylundecyl ammonium bromide ($Fc(C_{11})$) pH, temperature, H_2O_2 and $Fc(C_{11})$ concentrations were selected as parameters in order to investigate the Fenton reaction performance of the ferrocene bearing surfactant. First, experiments were carried out to show that Fenton reactions take place and MB removal was achieved as a result of the reaction. It is worth noting that the removal of MB was not affected by H_2O_2 or $Fc(C_{11})$ alone (**Figure 1**). However, when these two reagents were added to the medium, it was observed that the MB removal reached 100% over time. This suggests that the Fenton reaction can be successfully performed using the custom-designed surfactant $Fc(C_{11})$ and H_2O_2 together.

The effect of temperature (**Figure 2a**) and pH (Figure 2b) on the Fenton reaction was then investigated. The results indicate that temperature does not significantly affect the overall Fenton reaction from an application standpoint, as MB removal was close to 100% after 120 mins at all temperatures. Based on these experiments, the activation energy of the reaction was calculated to be 24.55 kJ/mol (Figure S1, Supporting Information). pH is one of the most critical factors in the Fenton reaction. The Fenton reaction appears to be most effective under acidic conditions, with an optimal pH of ≈3, regardless of the substrate.[33,34] Our experimental results indicate that MB removal was 100% at pH 2.5 and 90.3% at pH 4 at the end of 180 mins. At pH 5.5, the reaction does not take place significantly.

To investigate the effect of $Fc(C_{11})$ concentration experiments were performed with 0.5–4 mM $Fc(C_{11})$. The results showed that the reaction rate was slowest at 0.5 mm and increased with increasing concentrations up to 1 mM. However, concentrations above 1 mm did not significantly affect the reaction rate. The H_2O_2 concentration played critical role in the MB removal performance of the Fenton reaction. To determine the ideal hydrogen peroxide concentration, the reaction was performed with different H_2O_2 concentrations (Figure 2d). The %MB removal was determined to be 91.4%, 98.36%, 100%, and 100% for 6.93, 12.48, 18.03, and 23.58 mM concentrations at 180 min, respectively (Figure 2d). These findings suggest that higher concentrations of H_2O_2 may be more effective in removing MB compared to lower concentrations at each point throughout the reaction.

The ferrocenyl surfactant was used for the first time in the literature for this purpose. Experiments were conducted using scavengers to detect the radicals responsible for the removal of methylene blue (**Figure 3a**). NaN_3 was employed as an oxygen and OH radical scavenger,[35] while methanol as OH radical scavenger. It was observed that the MB removal decreased by 76% (down to 24%) in the presence of 20 mM NaN_3 which is the highest NaN_3 concentration studied, and the removal percentage of MB decreased down to 38.9%. The ESR spectra recorded at zero time

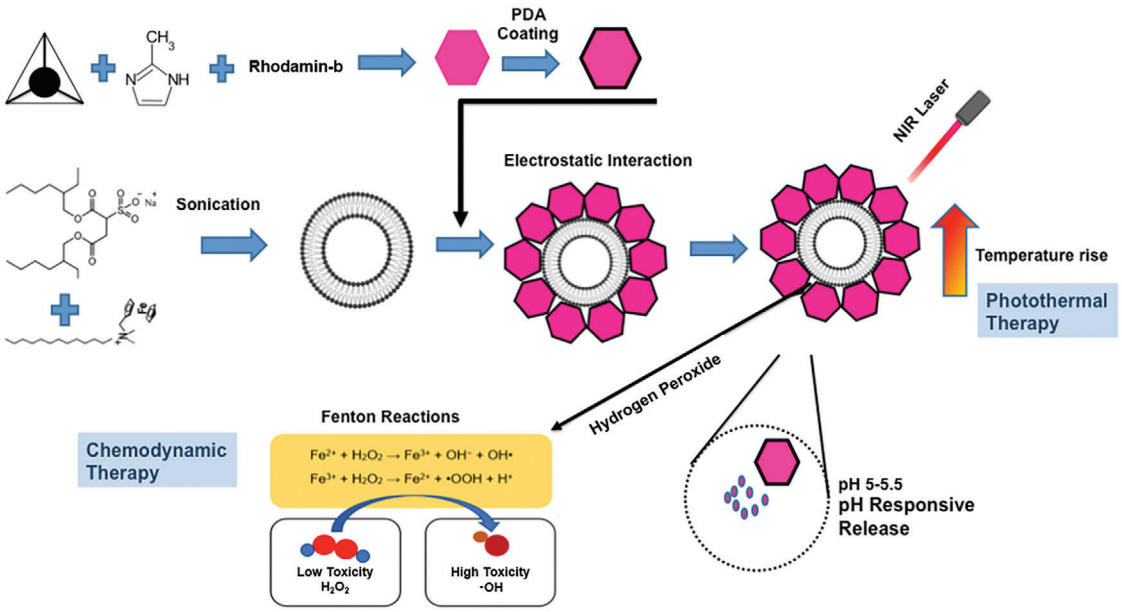

Scheme 1. Formation steps of Fc(C_{11})-AOT/Rhb@ZIF-8/PDA and schematic explanation of functions of the synergistic therapy agent. (Molecular structure of Fc(C_{11}) reprinted with permission from ref. [15]. Copyright 2024 Elsevier).

for the sample containing ferrocenyl surfactant was presented in Figure 3c. A comparison of the ESR spectra of Fc(C_{11}) recorded at 0 and 20 min, the peak-to-peak signal intensity of second signal denoted as "∗" was increased 1.18-fold. These results indicate that the reaction continued while the ESR spectra of the samples were recorded. This continuous performance of the reaction is attributed to the cyclic ability of the ferrocenyl surfactant as expected. It is worth noting that the ESR spectrum of the Fc sample consists of a group of three signals with relative intensity ratios of 1:1:1 and a distance of 15 G between them. The DMPO-$^1O_2$ radical is known to give an ESR spectrum with intensity ratios of 1:1:1 and a splitting constant of 15 G.[36] From this result, it was concluded that the radical formed in the sample having ferrocenyl surfactant during the reaction was DMPO$^{-1}O_2$. Fenton reactions are proposed to function through OH radical. However, different oxidant species are proposed to be formed depending on the reaction conditions such as pH, concentration, and redox potential. According to the literature, singlet oxygen ($^1O_2$) has been postulated as a highly reactive oxidant species.[37]

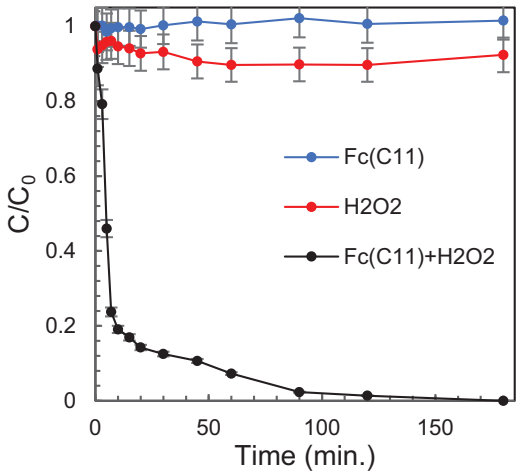

Figure 1. %MB discoloration efficiencies of Fc(C_{11}), H_2O_2 and Fc(C_{11})+H_2O_2 (23.58 mM H_2O_2, 1 mM Fc(C_{11}), 10 mg L^{-1} MB, pH 2.5, T = 37 °C). (All the experiments repeated at least three times).

In order to evaluate the possibility of reusing the ferrocenyl surfactant, the experiments were restarted by adding MB and hydrogen peroxide to the reaction medium at the end of every three hours. The findings indicate that the ferrocenyl surfactant remained efficient for minimum of five cycle (Figure 3b.), with complete removal of MB attained at the conclusion of each three-hour operation. In the first three cycles, there was no discernible change in the performance of the Fc(C_{11}) surfactant, with the majority of the MB being degreased within the first hour. However, following the third cycle, the required time to consume/decompose the MB to a similar extent was in the previous cycles increased to 160 min. It is important to note that 1 mM Fc(C_{11}) was used in this examination. The observed reduction in performance was considered to be related with change in the solution condition, as the chemical decomposition of MB results in a complex media. While the final products are carbon dioxide and water, the solution's composition is altered. As previously reported, cationic surfactant exhibits cyclic behavior of it (reduction/oxidation) that may result in slight performance loss when chemical reducing/oxidizing agents are used.

To provide a more accurate evaluation of the performance of the Fenton reactions, a kinetic evaluation of the data was conducted. In the literature, it has been seen that "pseudo first order" and "pseudo second order" kinetic models are applied to Fenton reactions and the reactions generally follow the "pseudo first order" model.[20,38,39] In this study, It was observed that the reaction followed a first-order kinetics at concentrations of 0.5 and 1 mM

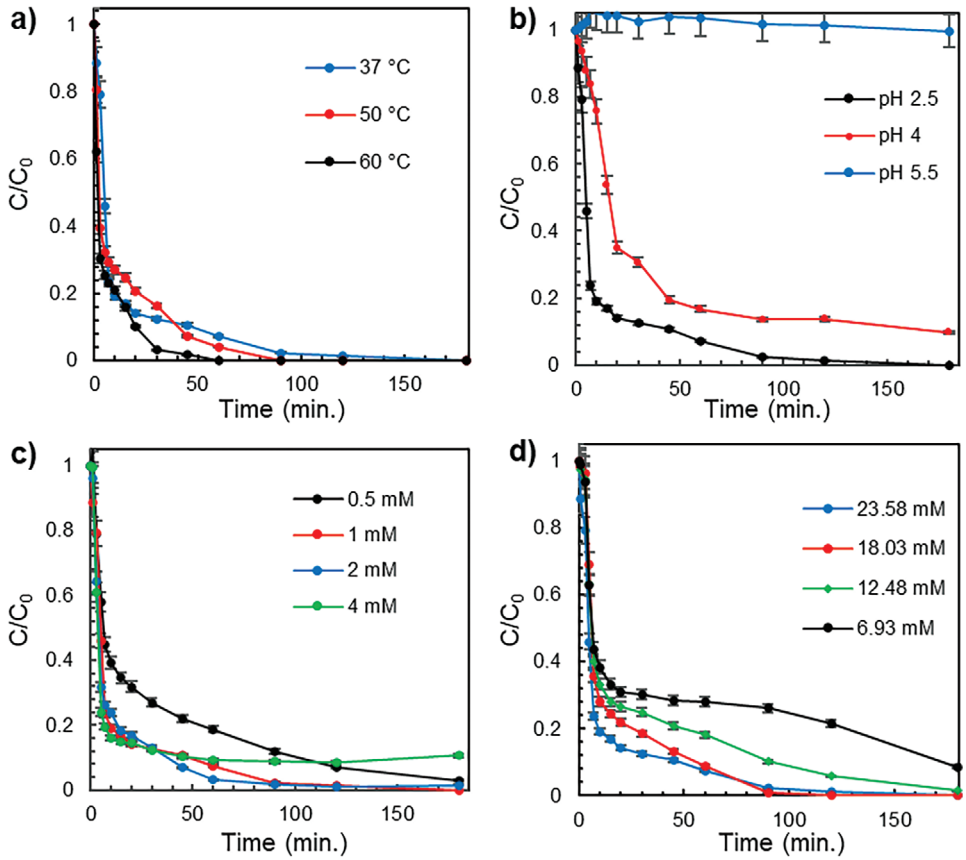

Figure 2. a) effect of temperature (1 mM $Fc(C_{11})$, 10 mg L^{-1} MB, pH 2.5, 23.58 mM H_2O_2), b) pH (1 mM $Fc(C_{11})$, 10 mg/L MB, T = 37 °C, 23.58 mM H_2O_2), c) $Fc(C_{11})$ (23.58 mM H_2O_2, 10 mg L^{-1} MB, pH 2.5, T = 37 °C) and d) H_2O_2 concentration (1 mM $Fc(C_{11})$, 10 mg/L MB, pH 2.5, T = 37 °C) (Measurements were repeated at least three times).

(Table S1, Supporting Information) with k values of 22.3×10^{-3} and 36.3×10^{-3} min^{-1} respectively. The observed increase in k value with increasing concentration of $Fc(C_{11})$ suggest that the ferrocenyl surfactant has a catalytic effect on the reaction. This finding is consistent with previous research by Wang et al., who calculated the k value of 26.02×10^{-3} for 1 mM ferrocene.[20] The results indicate that incorporating ferrocene as the head group of a surfactant does not have a negative impact on Fenton reaction performance. This will give the possibility of using other assembled structures such as vesicles as catalysts for Fenton reactions provided that $Fc(C_{11})$ surfactant is used as a component in the vesicles.

2.1. $Fc(C_{11})$-AOT Vesicle Preparation

After it was seen that the ferrocenyl surfactant could perform Fenton-like reactions, catanionic vesicles were prepared using AOT and $Fc(C_{11})$ through electrostatic interaction. The hydrodynamic radius of the vesicles was determined to be 198.20 ± 42.01 nm and 205.98 nm by DLS and SLS, respectively. The radius of gyration (R_g) of vesicles was also found to be 197.09 ± 1.12 nm. Static and dynamic light scattering data were evaluated together to obtain information about the geometries of the structures. The R_g/R_h (R_h is hydrodynamic radius) value can provide information about the geometry, with a value close to 1 indicating vesicular structures with a thin monolayer.[40] In this study, the ratio was determined to be 0.99. In addition, based on the SLS data, the particle scattering function which is characteristic of the particle shape was obtained using the Guiner model (**Figure 4**). Based on this model, the obtained structures appear to be consistent with the curve of the hard sphere. These data support the shape information obtained from the R_g/R_h ratio and indicate the presence of vesicles.

The redox sensitivity of the catanionic vesicles and their disintegration conditions were also investigated (Figure S2a,b, Supporting Information). It is known that vesicles can be disrupted with surfactants such as Triton X-100.[41] It has been reported in the literature that ferrous compounds such as ferrocene undergo a redox reaction with cerium sulfate $Ce(SO_4)_2$.[9] The color transition from yellow to blue-green during the ferrocene-ferrocenium reaction is very distinct, making it possible to track the reaction with UV-vis spectrophotometry. Addition of cerium sulfate to the vesicles caused the formation of a peak at 640 nm. The oxidation of ferrocene to ferrocenium resulted in the disappearance of the cloudy appearance of the vesicle dispersion. Upon the addition of Triton X-100, the UV–vis absorbance of the vesicle solution decreased, indicating the disintegration of the vesicles. Further investigation was carried out using DLS. The experiment revealed that upon adding Triton X-100 to the medium the size of the

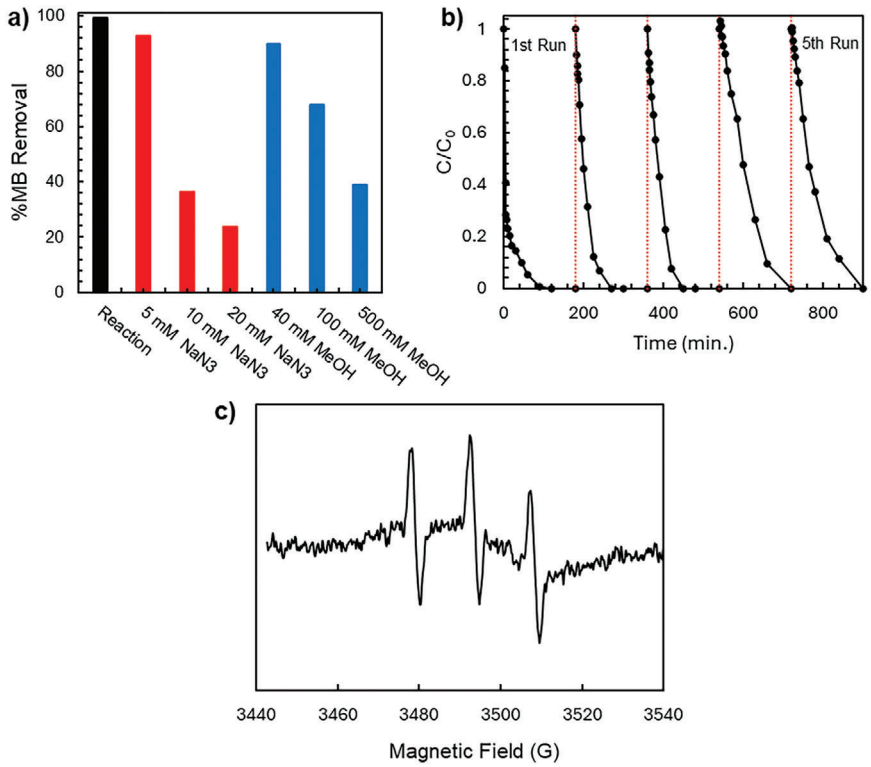

Figure 3. a) Effect of NaN_3 and MeOH on %MB removal (3 h reaction time, 1 mM Fc(C_{11}), 23.58 mM H_2O_2, pH 2.5, T = 37 °C) and b) reusability experiments for Fc(C_{11}) (Measurements were repeated at least three times) c) ESR spectrum of Fc(C_{11}) at time zero.

colloidal structures changed from 198.20 to 28.43 nm, leading to a transformation from vesicles to micelles.

2.2. Preparation and Characterization of ZIF-8, Rhb@ZIF-8 and Rhb@ZIF-8/PDA

Size analysis of the ZIF-8, Rhb@ZIF-8 and Rhb@ZIF-8/PDA crystals were carried out by using DLS, AFM, and TEM (**Table 1**). The DLS measurements indicated that the Rhb loading resulted an increase ≈20 nm on the size of ZIF-8 crystals (226.32 ± 49.52 nm). In addition, the PDA coating caused a 30 nm increase in size, resulting in Rhb@ZIF-8/PDA particles with a size of 276.84 ± 186.82 nm.

Table 1. Particle sizes of ZIF-8, Rhb@ZIF-8 and Rhb@ZIF-8/PDA particles.

Nanoparticle	PDI	LS [nm]	AFM [nm]	TEM [nm]
ZIF-8	0.43 ± 0.08	226.32 ± 49.52	92.33 ± 30.50	183.33 ± 126.00
Rhb@ZIF-8	0.37 ± 0.04	245.48 ± 160.56	149.37 ± 41.33	273.00 ± 38.11
Rhb@ZIF-8/PDA	0.40 ± 0.04	276.84 ± 186.82	205.28 ± 119.16	307.33 ± 78.00

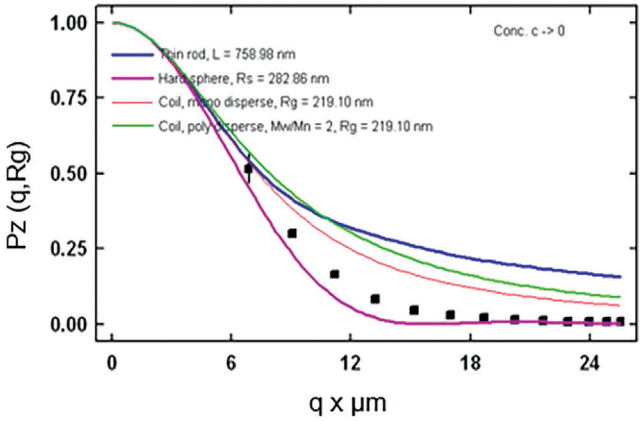

Figure 4. Comparison of the scattering function (P_θ) of Fc(C_{11}) (■)with the theoretical curves of different particle shapes (Measurements were repeated at least three times).

TEM (**Figure 5a–c**) and AFM (Figure S3, Supporting Information) yielded comparable outcomes. The crystal sizes of ZIF-8 exhibited an increase from 183.33 ± 126.00 nm to 273.00 ± 38.11 nm upon Rhb loading and to 307.33 ± 78.00 nm with PDA coating. TEM images were also showed that the PDA layer thickness was ≈15 nm, but the coating was not homogeneous.

XRD, one of the most powerful analytical techniques for investigating ZIF-8 crystals, was performed to investigate the effect of Rhb loading and PDA coating on the crystal (Figure 5d). Strong and sharp peaks at 2θ = 7.26, 10.32, 12.66, 14.64, and 16.38 and 17.97 belongs to (110), (200), (211), (220), (310), and (222) planes and showed that ZIF-8 nanoparticles with high crystallinity were successfully obtained. There was no change in the positions of the peaks and the peak intensities to each other upon

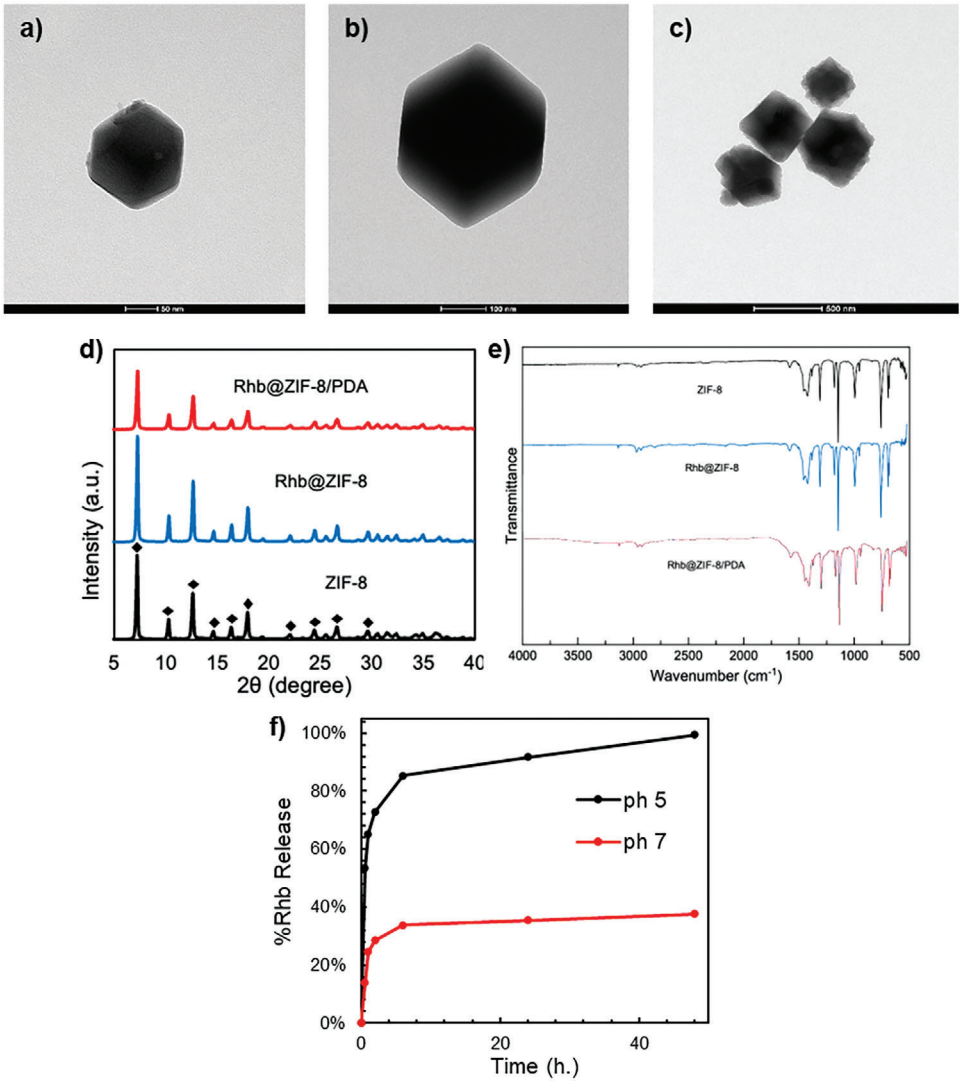

Figure 5. TEM images of a) ZIF-8, b) Rhb@ZIF-8 and c) Rhb@ZIF-8/PDA (1 h reaction), d) XRD patterns, e) FTIR spectra of ZIF-8, Rhb@ZIF-8, and Rhb@ZIF-8/PDA, f) the pH-responsive release of Rhb from Rhb@ZIF-8 (Measurements were repeated at least three times).

encapsulation of Rhb. However, a slight decrease in the peak intensity was observed with the PDA coating. It is worth noting that the effect of the PDA coating is highly dependent on the thickness of the PDA layer. For this reason, it is necessary to optimize the thickness of the PDA layer which should give an effective photothermal effect but also do not reduce the crystallinity of the ZIF-8 significantly. The thickness of the PDA layer can be adjusted by controlling the reaction time. For this study, a reaction time of 1 h was chosen since the temperature rise obtained by the PDA layer formed was satisfactory for PTT. Above this reaction time etching of the MOF structure because of possible complexation was reported to be significant in literature.[42] Figure 5e presents the FTIR spectra of ZIF-8, Rhb@ZIF-8 and Rhb@ZIF-8/PDA.The spectra reveal the presence of bending and stretching peaks in the imidazole ring, can be seen in the range of 500–1350 cm^{-1} and 1350–1500 cm^{-1}, respectively. The peaks at 3135 and 2929 cm^{-1} were attributed to aromatic and aliphatic C-H bonds.[42] There was no significant change in the FTIR spectrum was observed upon encapsulation of RhB or PDA coating, which corroborates our hypothesis that the ZIF-8 structure remained unaltered.

The Rhb EE% of the ZIF-8 crystals was determined to be 35.73. The release of rhodamine-b from ZIF-8 crystals was in PBS solutions at both 7.4 and pH 5 (Figure 5f). The results showed that ZIF-8 released Rhb at a much faster rate at pH 5 than at pH 7.4, with a significantly higher burst release of the RhB at low pH. Specifically, 73% of Rhb was released in the first two hours, this increased to 85% at the end of 6 h. The release was complete after 48 h, following a slow progression. However, under neutral conditions, the release only reached 28% in 2 h, 34% in 6 h, and 38% in 48 h. The amount of RhB released was higher than what we expected. The cause of this behavior is thought to be related to the stability of ZIF-8 in PBS media, as reported in the literature.[43] To address this issue, RhB release from ZIF-8 was tested in various environments, revealing that the concentration of PBS has an impact on the release of RhB. 1X PBS

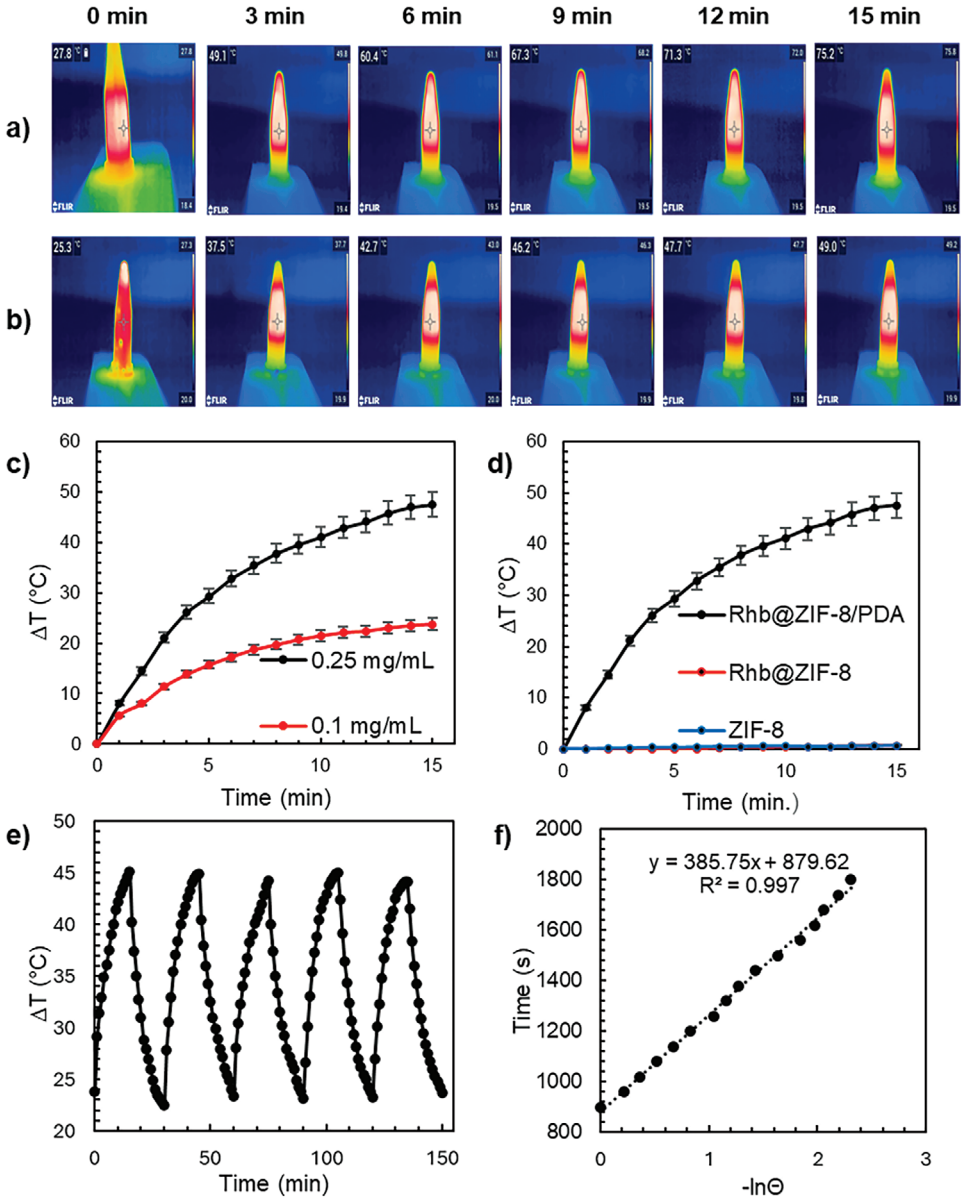

Figure 6. Thermal camera images of a) 0.25 mg mL^{-1} and b) 0.1 mg/mL Rhb@ZIF-8/PDA dispersion. Temperature changes of c) Rhb@ZIF-8/PDA particles at different concentrations and d) ZIF-8, Rhb@ZIF-8 and Rhb@ZIF-8/PDA particles at 0.25 mg mL^{-1} e) Photothermal stability of 0.1 mg ml^{-1} concentration of Rhb@ZIF-8/PDA particles under NIR irradiation f) Photo thermal conversion efficiency (808 nm λ, 1.5 w) (Measurements were repeated at least three times).

caused up to 34% release in 24 h whereas 0.1X PBS caused only 19% release (Figure S4, Supporting Information). The pH sensitivity of ZIF-8 crystals was thoroughly investigated through a release experiment involving a stepped pH change (Figure S5, Supporting Information). The results showed that ZIF-8 crystals released of 38% of RhB over 48 h at neutral pH and reached a plateau. Upon reducing the pH was reduced to 6, the amount of RhB release increased and reached to 58% with a 20% increase in 6 h. Further reduction of the pH to 5 resulted in almost complete release in 96 h.

2.3. Photothermal Effect of Rhb@ZIF-8/PDA

To observe the photothermal effect caused by the PDA layer, a NIR source with a wavelength of 808 nm was used and the temperature change was monitored with the help of a thermal camera (**Figure 6**a,b). The Rhb@ZIF-8/PDA was initially exposed to a laser with a power of 1.5 W for 15 min at a concentration of 0.25 mg mL^{-1}, resulting in a temperature increase of 47.4 °C (from 27.8 to 75.2 °C) during the exposure. The sample containing 0.1 mg mL^{-1} Rhb@ZIF-8/PDA experienced a

temperature increase of + 23.7 °C after 15 min of irradiation (Figure 6c). To further investigate the impact of the PDA coating more clearly, ZIF-8, Rhb@ZIF-8 and Rhb@ZIF-8/PDA particles at a concentration of 0.25 mg mL^{-1} were also irradiated to determine the cause of the observed temperature rise. The result of the photothermal experiments (Figure 6d) indicate that ZIF-8 and Rhb@ZIF-8 particles caused a temperature increase of only 0.7 °C in 15 min. It has been reported in the literature that this temperature increase is equivalent to the temperature increase of pure water.[44] Based on this, it can be concluded that ZIF-8 and Rhb@ZIF-8 particles do not exhibit a photothermal effect. The observed temperature increases with Rhb@ZIF-8/PDA dispersion was only attributed to the PDA layer.

After determining the sufficient concentration for photothermal therapy, the photothermal conversion efficiencies of Rhb@ZIF-8/PDA particles were calculated by analyzing heating-cooling cycles of 0.1 mg mL^{-1} Rhb@ZIF-8@PDA particles (Figure 6a). The particles were found to have a photothermal efficiency of 25.17% (Figure 6b).

2.4. Preparation of Fc(C_{11})-AOT/Rhb@ZIF-8/PDA Synergistic Therapy Agent

Fc(C_{11})-AOT vesicles and RhB loaded, PDA-coated ZIF-8 (Rhb@ZIF-8/PDA) were assembled through electrostatic interactions. Since the electrostatic interaction is the main contribution expected to give rise to the structure, we measured the zeta potential of Rhb@ZIF-8/PDA and Fc(C_{11})-AOT's. ZIF-8 has a zeta potential of +25.1 ± 0.48 mV, while Rhb@ZIF-8/PDA particles had a zeta potential of −19.86 ± 0.56 mV with the effect of the PDA coating. When the vesicles were synthesized at 1:1.5 AOT:Fc(C_{11}) ratio, their zeta potential was measured to be 28.76 ± 0.94 mV due to ferrocene.

The vesicle solution was mixed with the calculated amount of ZIF-8 required for the coating and incubated. The zeta potential of the coated vesicle approached that Rhb@ZIF-8/PDA (−19.86 mV) as the coating time increased (Table S2, Supporting Information). After 3 h, it was observed that the zeta potential of Fc(C_{11})-AOT/Rhb@ZIF-8/PDA was measured as −19.3 ± 0.5 mV which shows that the surface of the vesicles is covered with ZIF-8.

The size of the obtained structures was analyzed using AFM and DLS. As previously mentioned, the vesicles had a size of ≈400 nm according to the DLS analysis. The dimensions of the vesicles coated with Rhb@ZIF-8/PDA were found to be as large as 626.40 ± 50 nm. In the AFM analysis, the aqueous core of the vesicle, which collapsed as the samples dried, and a layer around it with a thickness ranging of 90–200 nm can be seen (**Figure 7**). It is thought that this layer belongs to the Rhb@ZIF-8/PDA particles and that the new tailored capsules retain their spherical shape even after drying. Upon drying, the aqueous core forms a region in the center that measures ≈300 nm, which is comparable to the size of uncoated vesicles. Because of the AFM is approaching the sample from top only upper part of the structure can be captured. As a result, we have determined that the dimensions of Rhb@ZIF-8/PDA coated Fc(C_{11})-AOT vesicles were determined were 541.75 ± 227.91 nm. SEM images of of Rhb@ZIF-8/PDA coated Fc(C_{11})-AOT vesicles can also be seen from Figure S6 (Supporting Information).

To develop a multi-purpose treatment agent with a synergistic effect, we compared the overall performance of the system with the performance obtained when its components were used separately. We evaluated the Fenton reaction performance by analyzing the percentage of MB removal via Fc(C_{11})-AOT/Rhb@ZIF-8/PDA that had an equivalent amount to 1 mM ferrocene surfactant in the reaction medium (**Figure 8a**). The microcapsule's Fenton reaction performance was comparable to that of the monomeric surfactant of Fc(C_{11}) and uncoated Fc(C_{11})-AOT vesicles. However, the vesicles perform the Fenton reaction more slowly than the monomers, which needs to be explained. One possible explanation is that some of the head groups of Fc(C_{11}) are located in the inner part of the bilayer of the vesicle that is not in contact with the hydrogen peroxide environment. To elucidate the observed performance, the ESR spectrum of Fc(C_{11})-AOT vesicles solution was taken at zero time and presented in Figure 8b. From the comparison of the ESR spectra of Fc(C_{11})-AOT sample recorded at 0 and 20 min, an increase in peak-to-peak signal intensity of the second resonance signal denoted as "↓"was observed as 3.85 fold (Figure S7, Supporting Information). It was extracted from the Figure 8b that the resonance signals denoted with arrows (↓) are separated by ∼15 G and have the relative signal intensity ratios of 1:2:2:1. These resonance signals have been attributed to the DMPO-OH radical which gives a sextet signals with splitting constants of $A_N = A_H = 15$.[36] The intensity of the resonance signals denoted as "∗" in Figure-8b have the same time variations and most probably originated from the same radical. These sextet signals have been observed in various studies and attributed to the DMPO-CH3 radical with $A_N = \approx 16$ and $A_H = \approx 23$ G.[36,45,46] The remaining resonance signals marked with "+" were separated by ≈15 G and seems as a partially resolved triplet signals with intensity ratios 1:1:1. These signals have been attributed to the two conformer of DMPO-$^1O_2$ radical which have slightly different A_N splitting constant.

To support the explanations provided, the simulation studies were carried out by using the non-linear square method and the subroutine program "fminsearch.m" operating on MATLAB. The data of the experimental ESR spectrum of the Fc(C_{11})-AOT sample given in Figure 8b was used in simulation calculations. Simulation studies were carried out based on DMPO-OH, DMPO-CH_3 and DMPO-$^1O_2$ radicals. However, in order to simulate the resolved signals indicated by "+", two different DMPO-$^1O_2$ radicals having slightly different hyperfine splitting constants were proposed instead of the DMPO-$^1O_2$ radical. It was observed from the simulation calculations that the experimental ESR spectrum of Fc(C_{11})-AOT sample (Figure 8b) has been described well by the model based on the radicals aforementioned above. The calculated parameters from the simulation for these radicals were given in Table S3 (Supporting Information). The calculated parameters for the proposed radicals are consistent with the parameters given in literature. The experimental ESR spectrum and its calculated counterpart by using the parameters given in Table S3 (Supporting Information) were presented in Figure 8b. As can be seen from the Figure 8b, the agreement between the experimental and theoretical ESR spectra is fairly good.

The percent removal performance of MB of vesicles coated with ZIF-8 was comparable to that of uncoated vesicles until the

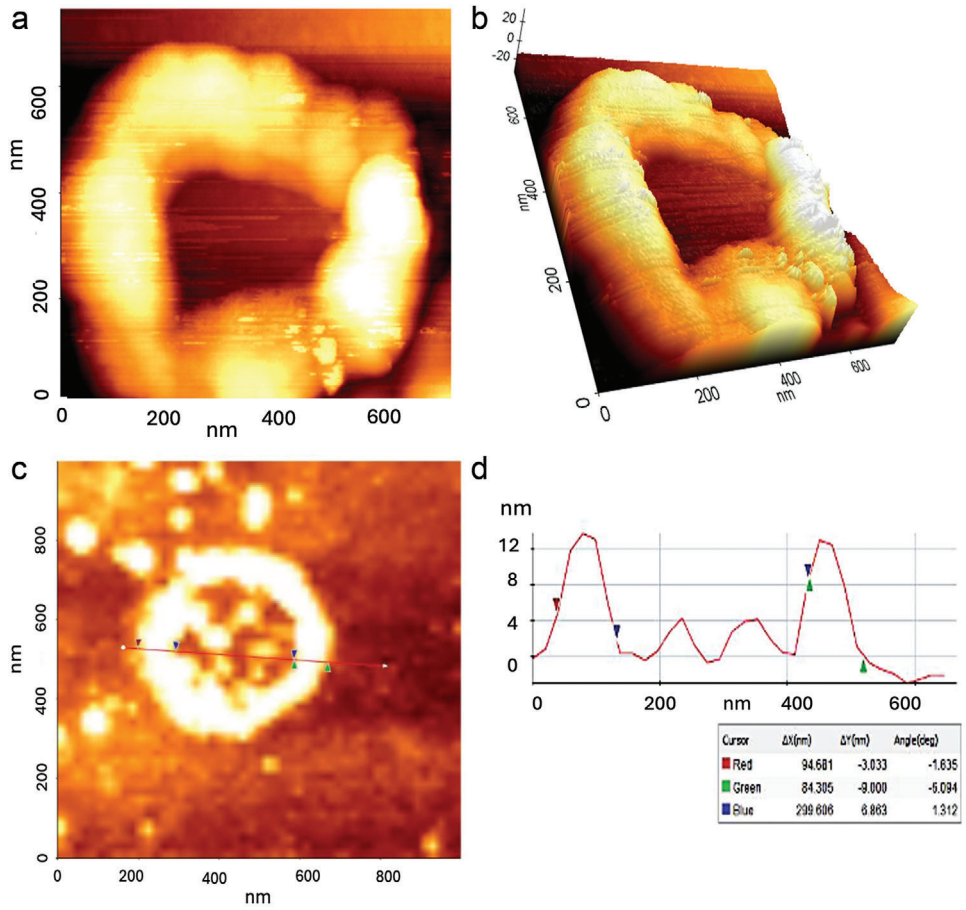

Figure 7. a,b) 3D and c) 2D topographic AFM images of Fc(C_{11})-AOT/Rhb@ZIF-8/PDA and d) line profile obtained from Fc(C_{11})-AOT/Rhb@ZIF-8/PDA.

15th min. Since the stability of ZIF-8 is quite low at these pHs, it was thought that it would degrade directly and there would be no layer on the surface to prevent the Fenton reaction sterically. However, the encapsulated RhB molecules released from ZIF-8 at low pH become available for the Fenton reaction and it is known that Rhb can be degraded by Fenton-like reactions in the presence of hydrogen peroxide.[47] Some of the hydroxyl radicals produced by the Fenton reaction could be used to remove RhB together with MB. This was given as the reason for the slower trend after the 15th min.

RhB release studies were also carried out at pH 5 to observe the difference in RhB release between Rhb@ZIF-8/PDA crystals and Fc(C_{11})-AOT/Rhb@ZIF-8/PDA (Figure 8c). In particular, the first one-hour release of RhB from was significantly lower compared to Rhb@ZIF-8/PDA. 61% of RhB was released from Rhb@ZIF-8/PDA over a one-hour period, whereas only 45% RhB release was observed from ZIF-8 coated vesicles. It was noted that the slower release might be due to the vesicle inhibiting acidic release environment, which comes into contact with the Rhb@ZIF-8/PDA particles. It was concluded that the Rhb@ZIF-8/PDA particle surface was partially adhered to the vesicle surface during the coating process, resulting in a reduced contact surface with the acidic medium. Rhodamine-b release from PDA-coated and uncoated ZIF-8 crystals was also compared to determine whether the PDA layer had any effect on the change in the release profile (Figure S8, Supporting Information). It was observed that PDA did not play a role in Rhb release. Therefore, it can be concluded that the change in the release profile is solely due to the reason mentioned above.

Finally, the photothermal efficiency of the system was investigated. No significant change was observed in the photothermal efficiency of the system was observed after coating (Figure 8d). The temperature increases generated by Rhb@ZIF-8/PDA and Fc(C_{11})-AOT/Rhb@ZIF-8/PDA in a 15 min. period were 23.8 and 22.9 °C, respectively. This was interpreted that the coating of Fc(C_{11})-AOT vesicles with Rhb@ZIF-8/PDA to did not cause any loss of photothermal performance.

3. Conclusion

A ferrocenyl surfactant-containing vesicle that successfully underwent Fenton reactions was produced in this study. This vesicle has the potential to induce tumor cell death through the hydroxyl radicals it generates and can also serve as a drug carrier reservoir in its core. Additionally, the vesicle is coated with a ZIF-8 that can efficiency load the model molecule Rhb (37% efficiency) and can be used for chemotherapy thanks to its pH-sensitive release mechanism. In addition, this system allows the temperature increase required for photothermal therapy by modifying of PDA on the ZIF-8 surface. Therefore, we designed and

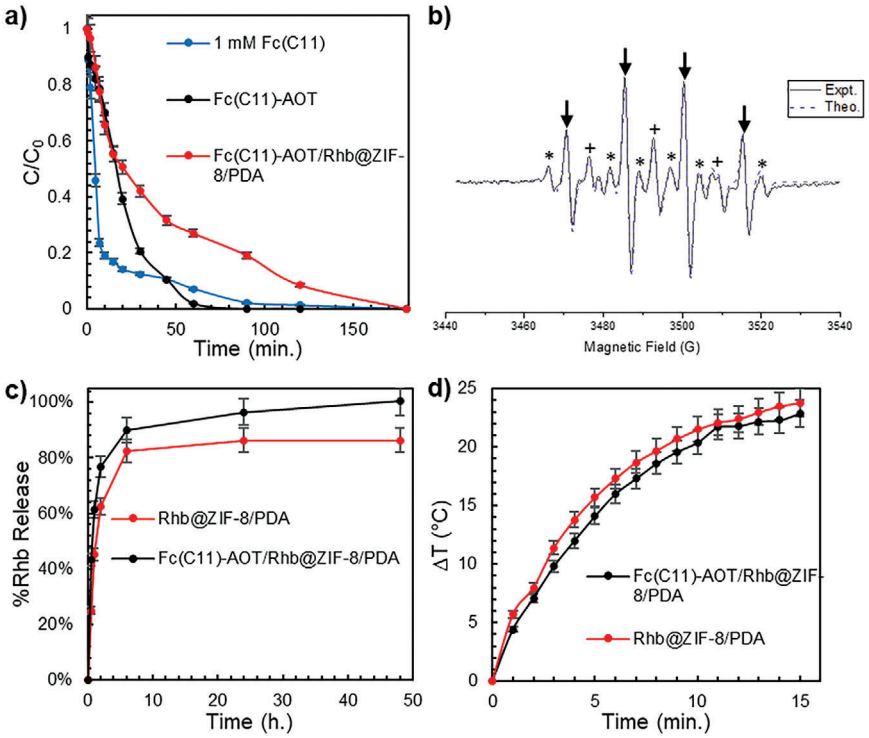

Figure 8. a) %MB removal performance of 1 mM Fc(C_{11}), Fc(C_{11})-AOT vesicle and Fc(C_{11})-AOT/Rhb@ZIF-8/PDA capsule (23.58 mM H_2O_2, pH 2.5 and T = 37 °C), b) ESR spectrum of Fc(C_{11})-AOT at time zero and comparison with theoretical calculations, c) RhB Release from Rhb@ZIF-8/PDA and Fc(C_{11})-AOT/Rhb@ZIF-8/PDA at pH 5 and d) Temperature rise of Rhb@ZIF-8/PDA and Fc(C_{11})-AOT/Rhb@ZIF-8/PDA under NIR irradiation (808 nm, 1.5 W) (Measurements were repeated at least three times).

produced Fc(C_{11})-AOT/Rhb@ZIF-8/PDA, which can function as a combined anticancer agent through chemotherapy, chemodynamic therapy and photothermal therapy as a combined anticancer agent. Further investigation need to be done and are planned for future studies including of in-vivo experiment for a selected disease model.

4. Experimental Section

Materials: Zinc nitrate hexahydrate, 2-Methylimidazole, sodium chloride, monosodium phosphate, dipotassium phosphate, dopamine hydrochloride, methanol and methylene blue were obtained from Sigma Aldrich (St. Louis, MO, USA). Triethylamine was purchased from Acros Organics (Carlsbad, CA, USA). Potassium Chloride was obtained from Merck (Darmstadt, Germany). All materials were used without further purification, and ultrapure water was used for all experiments.

Preparation of Fc(C_{11})-AOT Vesicles: Sodium dioctylsulfosuccinate (DOSS or AOT) and N,N-dimethylferrocenylmethylundecyl ammonium bromide (Fc(C_{11})) were used in the preparation of vesicles. (Fc(C_{11})) was synthetized as described previously.[48] 5 mM aqueous AOT and Fc(C_{11}) solutions in water were prepared in separate containers. Then these two solutions were mixed at a molar ratio of 1:1.5 for 1 h with sonication. After the vesicle dispersion is obtained, it is taken into a dialysis membrane to separate the monomers from the vesicle solution and dialyzed to water overnight.

Preparation of Rhb@ZIF-8: In this study, Rhodamin-b (Rhb) was used as a model molecule for small molecule weight drugs as well as a fluorescence probe. Rhb loaded ZIF-8 was prepared based on the work of Abdelhamid et al with small modifications.[49] Briefly, 0.2 g $Zn(NO_3)_2{\cdot}6H_2O$ was dissolved in 0.8 ml water and 0.2 ml of triethylamine (TEA) and 4 ml of Rhb solution (8 µM) were added to this solution sequentially. Another solution was prepared by dissolving 1.1 g 2-methyl imidazole in 4.4 ml water. After the zinc solution was mixed for 1 min, imidazole solution was added dropwise to zinc solution. Then the volume was completed to 24 ml with water and the reaction mixture was stirred for 15 min. All solutions were prepared using water. The final product was collected using centrifugation (13000 rpm, 20 min) and washed using 1:1 ethanol:water. All products were dried for 24 h in an oven at 80 °C.

PDA Coating on ZIF-8 Surface: First, 10 mM Tris buffer solution for use in PDA coating was prepared (pH = 8.5). The Rhb@ZIF-8 particles were then dispersed in Tris solution at a concentration of 1 mg mL^{-1}. The tris solution of dopamine hydrochloride was added to this solution as 1:1 by weight of Rhb@ZIF-8:Dopamin HCl. This mixture was stirred in the dark for 1 h. It was centrifuged at 10000 rpm for 6 min and washed twice with water. The resulting product was dried at 50 °C for 24 h.

Assembling Rhb@ZIF-8/PDA and Fc(C_{11})-AOT Vesicles: Electrostatic interactions were used to assemble the resulting vesicle and ZIF-8 compartments. The aqueous dispersion of Rhb@ZIF-8/PDA and AOT-Fc(C_{11}) vesicles were incubated for 1 h to obtain the drug delivery system. Then, for separation of the uncoated Rhb@ZIF-8/PDA the sample was centrifuged at 5000 rpm for 6 min.

pH-Dependent Release of Model Molecule Rhb

Release systems were prepared by suspending 1 mg Rhb@ZIF-8, Rhb@ZIF-8/PDA and Fc(C_{11})-AOT/Rhb@ZIF-8/PDA equivalent to 1 mg Rhb@ZIF-8/PDA materials in 1 mL of PBS solutions (pH 7.4 and 5.0) at 37 °C. Release mediums were sampled at every time point and UV–vis spectrophotometer was used to measure the absorbance at 554 nm to determine the amount of released Rhb.

Catalytic Activity Evaluation of Ferrocenyl Surfactant: The methylene blue (MB) removal method[35] was used to determine the catalytic activity of the ferrocene surfactant. All experiments were carried out in a volume of 2.5 mL solution. pH values were adjusted using dilute HCl. The

Fenton reaction started with the addition of hydrogen peroxide and samples were taken at each time point and analyzed by UV–vis spectrophotometer. The reusability of the Fc(C_{11})-AOT/Rhb@ZIF-8/PDA was investigated by adding MB and H_2O_2 after each run was completed. The color change was monitored over time via UV–vis spectrophotometer. Scavenger like methanol and sodium azide was utilized to elucidate the mechanism of MB removal. In addition, ESR measurements were carried out by using Bruker EMX 131 X-Band ESR Spectrometer (Germany) operating at a frequency of 9.806 GHz, a microwave power of 16.0 mW and modulation amplitude of 2.0 G. The scan range and time constant were adjusted as 100 G and 40.96 ms, respectively. To increase the signal to noise ratio, all ESR spectra were recorded 5 times consecutively. ≈3 min after the reaction starts, both the Fc(C_{11}) and Fc(C_{11})-AOT samples were transmitted to the capillary tubes of inner diameter 1 mm. Then, the capillary tubes were inserted to a quartz tube of inner diameter 3 mm which was placed in the sample cavity of the ESR Spectrometer. The ESR spectra of both the Fc(C_{11}) and Fc(C_{11})-AOT samples were recorded with the same spectrometer operating conditions at specific times of 0, 5, 10, 15, and 20 min after tuning the spectrometer. It must be emphasized that during this period, the position of the samples in the cavity was not changed.

Photothermal Analysis: 808 nm NIR laser and infrared camera were used to examine the photothermal effects of Rhb@ZIF-8/PDA and Fc(C_{11})-AOT/Rhb@ZIF-8/PDA. Samples irradiated with an NIR laser (1.5 W) and temperature of the samples was monitored by an infrared camera. Photothermal conversion efficiencies were calculated by using the Equations S1–S4 (Supporting Information).[50]

All the experiments repeated at least three times unless it is stated. The standard deviation was calculated using the results of at least three different measurements.

Characterization of ZIF-8: XRD powder patterns were acquired on Rigaku Ultima IV. X-ray diffractometer using Cu Kα radiation at a scan rate of 0.05°/s. Size and morphology of nanocrystals were determined by transmission electron microscopy (TEM). Images were obtained using FEI 120 kV CTEM. Also, the size of ZIF-8 crystals measured with Malvern CGS-3 model light scattering device with 632.8 nm wavelength at 90° scan angle for six DLS runs. Atomic force microscopy (AFM) measurements were carried out at 0.3 Hz scanning rate using PSIA Corporation XE-100E device. Zeta potentials were recorded using the Zeta Meter System 3.0 and measurements repeated three times for each sample. FTIR spectrum of samples was taken to verify the chemical structure of the MOF.

Characterization of Vesicle: Size and shape of vesicles were determined using dynamic (DLS) and static light scattering (SLS) techniques. DLS measurements were carried out at 90° scan angle and at 37 °C temperature. SLS measurements were carried out at scanning angles of 30–150° with 10° intervals. Also, zeta potential measurements and AFM scans of vesicles were carried out by using the same procedure with ZIF-8 characterization.

Supporting Information

Supporting Information is available from the Wiley Online Library or from the author.

Acknowledgements

E.U acknowledges the scholarship awarded by the Scientific and Technical Research Council of Turkey (TUBITAK) 2210-C program.

Conflict of Interest

The authors declare no conflict of interest.

Data Availability Statement

The data that support the findings of this study are available from the corresponding author upon reasonable request.

Keywords

drug delivery systems, fenton reactions, synergistic therapy, vesicle, zeolitic imidazolate framework-8

Received: February 22, 2024
Revised: May 26, 2024
Published online: June 22, 2024

[1] L. Gao, Q. Chen, T. Gong, J. Liu, C. Li, *Nanoscale* **2019**, *11*, 21030.
[2] W. Fan, B. Yung, P. Huang, X. Chen, *Chem. Rev.* **2017**, *117*, 13566.
[3] M. Chang, Z. Hou, M. Wang, C. Li, J. Lin, *Adv. Mater.* **2021**, *33*, 2004788.
[4] J. Conde, N. Oliva, Y. Zhang, N. Artzi, *Nat. Mater.* **2016**, *15*, 1128.
[5] L. Sercombe, T. Veerati, F. Moheimani, S. Y. Wu, A. K. Sood, S. Hua, *Front Pharmacol* **2015**, *6*, 00286.
[6] P. Liu, G. Chen, J. Zhang, *Molecules* **2022**, *27*, 1372.
[7] D. Chen, X. Liu, X. Lu, J. Tian, *Front Pharmacol* **2023**, *14*, 1111991.
[8] B. Okmen Altas, G. D. Kalaycioglu, S. Lifshiz-Simon, Y. Talmon, N. Aydogan, *Mol. Pharmaceutics* **2024**, *21*, 633.
[9] Q. Li, X. Chen, B. Jing, Y. Zhao, F. Ma, *Colloids Surf. A* **2010**, *355*, 146.
[10] C. Ornelas, D. Astruc, *Pharmaceutics* **2023**, *15*, 2044.
[11] C. Swearingen, J. Wu, J. Stucki, A. Fitch, *Environ. Sci. Technol.* **2004**, *38*, 5598.
[12] X. R. Xu, H. B. Li, W. H. Wang, J. D. Gu, *Chemosphere* **2004**, *57*, 595.
[13] S. Koo, O. k. K. Park, J. Kim, S. I. Han, T. Y. Yoo, N. Lee, Y. G. Kim, H. Kim, C. Lim, J. S. Bae, J. Yoo, D. Kim, S. H. Choi, T. Hyeon, *ACS Nano* **2022**, *16*, 2535.
[14] Y. Wang, F. Gao, X. Li, G. Niu, Y. Yang, H. Li, Y. Jiang, *J Nanobiotechnology* **2022**, *20*, 69.
[15] N. Aydogan, C. A. Rosslee, N. L. Abbott, *Colloids Surf. A* **2002**, *201*, 101.
[16] N. Aydogan, N. L. Abbott, *Langmuir* **2001**, *17*, 5703.
[17] N. Aydogan, N. L. Abbott, *J. Colloid Interface Sci.* **2001**, *242*, 411.
[18] N. Aydogan, N. L. Abbott, *Langmuir* **2002**, *18*, 7826.
[19] H. Zhao, T. Li, C. Yao, Z. Gu, C. Liu, J. Li, D. Yang, *ACS Appl. Mater. Interfaces* **2021**, *13*, 6034.
[20] Q. Wang, S. Tian, P. Ning, *Ind. Eng. Chem. Res.* **2014**, *53*, 643.
[21] A. Eivazi, B. Medronho, B. Lindman, M. Norgren, *Polymers* **2021**, *13*, 589.
[22] G. D. Kalaycioglu, N. Aydogan, *Colloids Surf. A* **2020**, *584*, 124037.
[23] V. F. Yusuf, N. I. Malek, S. K. Kailasa, *ACS Omega* **2022**, *7*, 44507.
[24] B. Maranescu, A. Visa, *Int. J. Mol. Sci.* **2022**, *23*, 4458.
[25] H. Zheng, Y. Zhang, L. Liu, W. Wan, P. Guo, A. M. Nyström, X. Zou, *J. Am. Chem. Soc.* **2016**, *138*, 962.
[26] S. Hui, Q. Liu, Y. Han, L. Zhang, J. Yang, S. Jiang, H. Qian, W. Yang, *J. Mater. Chem. B* **2021**, *9*, 9961.
[27] Y. Li, J. Jin, D. Wang, J. Lv, K. Hou, Y. Liu, C. Chen, Z. Tang, *Nano Res.* **2018**, *11*, 3294.
[28] P. Yang, Y. Tian, Y. Men, R. Guo, H. Peng, Q. Jiang, W. Yang, *ACS Appl. Mater. Interfaces* **2018**, *10*, 42039.
[29] B. Liu, F. Hu, J. Zhang, C. Wang, L. Li, *Angew Chem Int Ed Engl* **2019**, *58*, 8804.
[30] L. Zhang, S. S. Wan, C. X. Li, L. Xu, H. Cheng, X. Z. Zhang, *Nano Lett.* **2018**, *18*, 7609.
[31] J. C. Yang, Y. Shang, Y. H. Li, Y. Cui, X. B. Yin, *Chem. Sci.* **2018**, *9*, 7210.
[32] Y. Wang, D. Wang, J. Wang, C. Wang, J. Wang, Y. Ding, Y. Yao, *Chem. Commun.* **2022**, *58*, 1689.
[33] A. Babuponnusami, K. Muthukumar, *J. Environ. Chem. Eng.* **2014**, *2*, 557.

[34] B. Okmen Altas, C. Goktas, G. Topcu, N. Aydogan, *ACS Appl. Mater. Interfaces* **2024**, *16*, 15533.
[35] Q. Wang, S. Tian, J. Cun, P. Ning, *Desalination and Water Treatment* **2013**, *51*, 5821.
[36] G. R. Buettner, *Free Radic Biol Med* **1987**, *3*, 259.
[37] P. Salgado Mendoza, V. Melin, D. Contreras, Y. Moreno, H. Mansilla, *J. Chil. Chem. Soc.* **2013**, *58*, 2096.
[38] K. Cui, H. Yi, Z. i. Zhou, Q. Zhuo, Y. Bing, Q. Guo, Z. Xu, *Environ. Eng. Sci.* **2014**, *31*, 217.
[39] Y. Alegría, F. Liendo, O. Nuñez, *ARKIVOC: archive for organic chemistry*, **2003**.
[40] N. Aydogan, N. Aldis, *Langmuir* **2006**, *22*, 2028.
[41] D. Lichtenberg, H. Ahyayauch, F. M. Goñi, *Biophys. J.* **2013**, *105*, 289.
[42] E. Uysal, *Master's Thesis*, Hacettepe University, Turkey, **2023**.
[43] A. S. Spitsyna, A. S. Poryvaev, N. E. Sannikova, A. A. Yazikova, I. A. Kirilyuk, S. A. Dobrynin, O. A. Chinak, M. V. Fedin, O. A. Krumkacheva, *Molecules* **2022**, *27*, 3240.
[44] C. E. Okuyucu, G. D. Kalaycioglu, D. Kacaroglu, A. K. Ozden, N. Aydogan, *Colloids Surf. A* **2023**, *672*, 131763.
[45] I. Yamazaki, L. H. Piette, *J. Am. Chem. Soc.* **1991**, *113*, 7588.
[46] K. J. Reszka, M. L. McCormick, G. R. Buettner, C. M. Hart, B. E. Britigan, *Nitric Oxide* **2006**, *15*, 133.
[47] L. Liang, L. Cheng, Y. Zhang, Q. Wang, Q. Wu, Y. Xue, X. Meng, *RSC Adv.* **2020**, *10*, 28509.
[48] N. Aydogan, C. Rosslee, N. Abbott, *Colloids Surf., A* **2002**, *201*, 101.
[49] H. N. Abdelhamid, Z. Huang, A. M. El-Zohry, H. Zheng, X. Zou, *Inorg. Chem.* **2017**, *56*, 9139.
[50] X. Liu, B. Li, F. Fu, K. Xu, R. Zou, Q. Wang, B. Zhang, Z. Chen, J. Hu, *Dalton Trans.* **2014**, *43*, 11709.